UTC Report: Infrastructure Monitoring for Gradual Damage Detection From an In-service Light Rail Vehicle

Jacobo Bielak[1,*], Hae Young Noh[1,+], Mario Bergés[1,+], James H. Garrett[1], Jelena Kovačević[2,-], and Jingxiao Liu[1]

[1]Department of Civil and Environmental Engineering, Carnegie Mellon University, Pittsburgh, PA, 15213. [2]Department of Electrical and Computer Engineering, Carnegie Mellon University, Pittsburgh, PA, 15213.
[*]Principal Investigator: jbielak@cmu.edu
[+]Co-Principal Investigator
[-]Jelena Kovačević performed this work while she was with the Department of Electrical and Computer Engineering, Carnegie Mellon University; she is currently with Tandon School of Engineering, New York University.

FINAL RESEARCH REPORT

Contract No. DTRT-13-GUTC-26

1 Summary

The private freight rail industry makes $9.7 billion capital investment in maintaining the network, which is comprised of almost 140,000 miles of track and over 100,000 bridges in 2015. However, the Federal Railroad Administration still reported 1,096 derailments including 428 track caused accidents in the nation in 2017. This makes apparent the need for monitoring rail networks and railway bridge conditions. Recently, we introduced an indirect structural health monitoring approach which uses sensors on the vehicle to detect infrastructure changes and damage for low-cost maintenance. The ultimate objective of this project is to develop a system that would provide continuous monitoring of bridges and rail tracks by collecting vibration data from sensors on in-service trains. Ideally, such a system would be able to detect, localize and quantify the damage of tracks soon after they begin to occur.

To achieve the goal, we organized this problem into three tasks, starting with quantifying and localizing gradual damage on a laboratory model (section 3), followed by describing the DR-Train dataset collected from in-service trains over the past five years (section 4), and proposing a novel anomaly detection approach for monitoring longitude elevation of track geometry after revisiting the DR-Train dataset (section 5). The first task allows us to understand how the vehicle responds to an infrastructure with gradual damage; the second task provides us with a comprehensive understanding of our test-bed and dataset; and the third task takes a step forward to achieving the indirect monitoring in the real-world dataset.

Task 1: Supported by the University Transportation Center (UTC) at CMU, we have conducted lab-scale experiments and provided evidence of the applicability of the indirect damage diagnosis approach. Specifically, we introduced a physical-insight-based data-driven framework for comparing and estimating damage severity and location using only vibration signals collected from vehicles. By studying the physical insight of the vehicle dynamics, we achieved indirect gradual damage diagnosis in an unsupervised or a semi-supervised way. Further study is required to validate the robustness of this damage diagnosis framework with a more complex and realistic system. For instance, on-site tests are needed to verify the feasibility of this work in practice, and we also need to study the influence of different types of damage scenarios, vehicle velocity, ongoing traffic, and environmental factors.

Task 2: We published the DR-Train dataset, an open-access dataset recording dynamic responses from two in-service light rail vehicles that run on a 42.2-km light rail network in the city of Pittsburgh, Pennsylvania (USA). The DR-Train dataset also contains GPS positions and environmental data (including temperature, wind, weather, and precipitation) as the vehicles were running on the track and the track maintenance logs from the light-rail operator. The data were recorded from two light rail vehicles for four years with a variety of influential factors. This dataset could be used for comparing different vibration-based damage diagnosis algorithms, validating signal processing methods, investigating environmental influences on train responses, etc.

Task 3: Currently, revisiting the DR-Train dataset has allowed us to propose a learning-based anomaly detection approach for monitoring longitude elevation of track geometry from the dynamic response of an in-service train. The proposed method uses a variational autoencoder (VAE) to detect the anomaly. The VAE takes accelerations as input and learns a mapping from the frequency-domain of accelerations to a low-dimensional latent space that represents the distribution of the observed data. After the model is calibrated, the reconstruction probability of the input data is used as an anomaly score for indicating how well the input follows the normal pattern. Our proposed approach outperforms two widely used supervised baseline models, a logistic regression model (Baseline) and a fully-connected neural network (NN-Feature), in terms of recall, precision, and F1-score. The results make the proposed indirect structural health monitoring approach a strong candidate for low-cost and frequent track geometry inspection.

Over the year, one journal paper and one peer-reviewed conference paper have been submitted and are under review, one dataset has been published, another journal paper has been drafted. Also, this grant has helped us to deploy vibration sensors on the Panhandle bridge, and we have been collecting data for validating our indirect damage diagnosis approaches in practice.

Contents

2 List of Papers, Dataset, and Presentations

Papers

Liu J., Chen S., Noh H. Y., Bielak J., Garrett J. H., Kovačević J., and Bergés M., Diagnosis for Indirect Structural Health Monitoring of a Bridge Model, Manuscript, 2018.

Liu J., Chen S., Lederman G., Kramer D. B., Noh H. Y., Bielak J., Garrett J. H., Kovačević J., and Bergés M., Dynamic responses, GPS positions and environmental conditions of two light rail vehicles in Pittsburgh, Nature: Scientific Data, Submitted, 2018.

Liu J., Noh H. Y., Bielak J., Garrett J. H., Kovačević J., and Bergés M., A Damage Localization and Quantification Algorithm for Indirect Structural Health Monitoring of Bridges Using Multi-Task Learning, AIP Conference Proceedings, Under Review, 2018.

Dataset

Liu J., Chen S., Lederman G., Kramer D. B., Noh H. Y., Bielak J., Garrett J. H., Kovačević J., and Bergés M., The DR-Train dataset: dynamic responses, GPS positions and environmental conditions of two light rail vehicles in Pittsburgh (Version 1.0.0). Zenodo, 2018. http://doi.org/10.5281/zenodo.1432702

Presentations

Liu J., "Damage Diagnosis Algorithms for Indirect Structural Health Monitoring of Bridges", PIANC-SMART Rivers Conference, Pittsburgh, PA, 2017. Poster Presentation.

Liu J., "A Damage Localization and Quantification Algorithm for Indirect Structural Health Monitoring of Bridges Using Multi-Task Learning", Engineering Mechanics Institute Conference, Boston, MA, 2018. Conference Presentation.

Liu J., "A Damage Localization and Quantification Algorithm for Indirect Structural Health Monitoring of Bridges Using Multi-Task Learning", Machine Learning in Science and Engineering, PA, 2018. Poster Presentation.

Liu J., "A Damage Localization and Quantification Algorithm for Indirect Structural Health Monitoring of Bridges Using Multi-Task Learning", 45th Annual Review of Progress in Quantitative Nondestructive Evaluation, Burlington, VT, 2018. Conference Presentation.

3 A Damage Localization and Quantification Algorithm for Indirect Structural Health Monitoring of Bridges Using Multi-Task Learning[1]

3.1 Introduction

The 2017 National Bridge Inventory of the Federal Highway Administration found that 47,619 out of 615,002 bridges in the U.S. were in poor condition across the nation [1]. For instance, Of Pennsylvania's more than 22,660 bridges, 23% are considered structurally deficient [2]. This makes apparent the need for monitoring the bridge condition. In this paper, we focus on developing a damage diagnosis algorithm for estimating both the location and magnitude of damage occurring on an experimental bridge.

Recently, there is a trend to establish monitoring systems on bridges by indirectly leveraging sensors on a passing vehicle. This approach has gained great popularity because of its low cost and low maintenance. In 2005, Yang et al. [3] proposed the indirect approach to detect the bridge damage information by modeling the vehicle-bridge interaction (VBI) system and extracting bridge frequencies from the dynamic response of a passing vehicle. Over the past decade, many researchers have proposed novel methods in this field, which can be divided into two categories depending on whether or not they rely on modal parameters [4]. Natural frequency-based methods [3, 5, 6, 7] are only able to do damage detection, while the methods of identifying the mode shapes of a bridge [8, 9, 10] can do damage detection and localization. In addition, although the non-modal parameter-based methods, such as signal processing and machine learning techniques [11, 12, 13, 14, 15], perform well in indicating bridge damage and have the potential to quantify the severity, these methods lack robustness to noise and require more physical insights for model selection and performance improvement. Figure 1 shows the procedure of the non-modal parameter-based method for indirect bridge structural health monitoring.

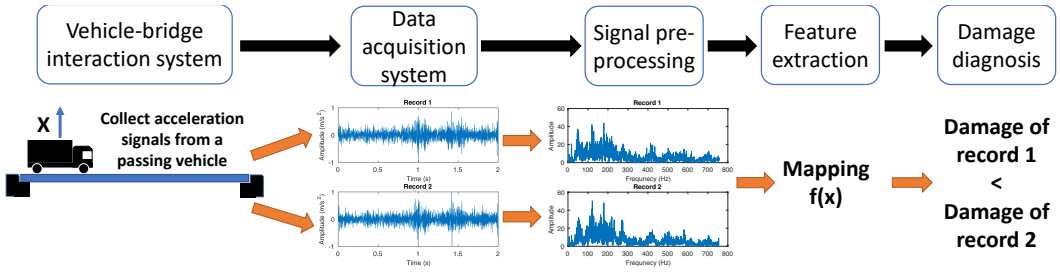

Figure 1. The procedure of the non-modal parameter-based method for the indirect bridge structural health monitoring system. Acceleration signals collected from a moving vehicle are pre-processed and inputted to a feature extraction system (learning a feature mapping from the spectrum or spectrogram of signals), and then the extracted features are used for damage diagnosis.

In our study, we propose a semi-supervised damage diagnosis algorithm using multi-task learning (MTL), which aims at estimating the damage locations and severity levels simultaneously by using acceleration signals collected from a vehicle passing over a bridge. We first derive the theoretical formulation of the VBI system with a mass attached at di erent locations on the bridge (representing damage severity) and show the nonlinear property of the dynamic response of the passing vehicle. The derivation also informs us that we must localize and estimate the severity mass simultaneously so that to minimize the uncertainty propagating from the location estimation. Hence, our MTL model uses non-linear activation functions and learns three tasks, namely feature extraction, damage location, and damage severity regression, simultaneously. A lab-scale experiment, an instrumented vehicle passing over an experimental aluminum bridge, is conducted for evaluating our model. The results show that our model can estimate locations of

[1]This work is based on the manuscript: Liu J., Noh H. Y., Bielak J., Garrett J. H., Kovačević J., and Bergés M., A Damage Localization and Quantification Algorithm for Indirect Structural Health Monitoring of Bridges Using Multi-Task Learning, AIP Conference Proceedings, Under Review, 2018.

the damage with an accuracy of 0.08 m (3.30% of the total length of the bridge) and changes in severity level with an accuracy of 17.81 grams (8.9% of the maximum severity mass). We also compare our MTL model with a two-step model which performs damage localization and severity estimation step-by-step and show that uncertainty propagating from location estimation affects the accuracy of damage diagnosis.

3.2 Numerical Solution of the Vehicle-Bridge Interaction System

To help inform our choice of statistical analysis methods used to analyze acceleration records collected from real-world experiments, we revisit the theoretical formulation derived by Yang et al. [3]. Figure 2 shows a one degree-of-freedom oscillator moving over a simply-supported beam. We assume the beam is of the Euler-Bernoulli type with constant cross sections. Under this assumption, there is no friction force between the 'wheel' and the beam. The damage is simulated by attaching a mass (m_s) at different locations of the beam (L_s).

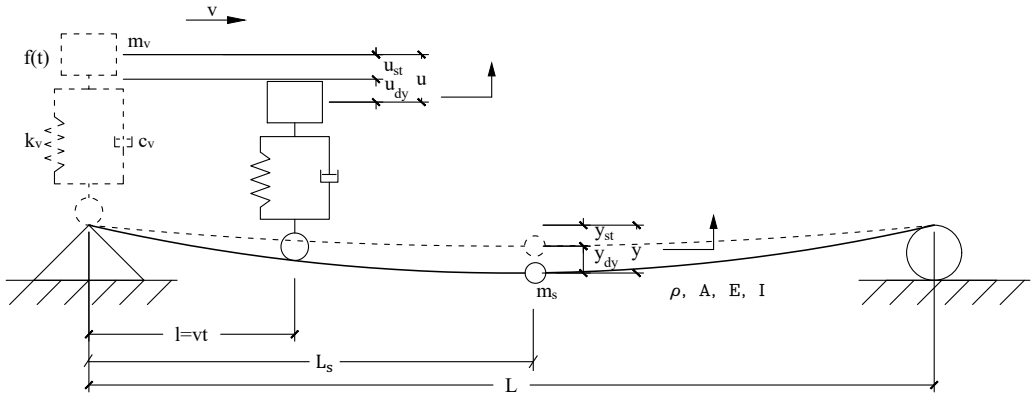

Figure 2. Simple vehicle-bridge interaction system with a mass attached at different locations.

The equations of motion for the vehicle and bridge are:

$$\begin{aligned} m_v\ddot{u}_{dy}(t) &+ k_v[u_{dy}(t) - y_{dy}(x=vt,t) - y_{st}(x=vt)] \\ &+ c_v[\dot{u}_{dy}(t) - \dot{y}_{dy}(x=vt,t) - \dot{y}_{st}(x=vt)] + f(t) = 0 \end{aligned} \tag{1}$$

$$\begin{aligned} \rho A\ddot{y}_{dy}(x,t) + m_s\ddot{y}_{dy}(L_s,t)\delta(x-L_s) + EIy''''_{dy}(x,t) = \{ &- m_v g \\ &+ k_v[u_{dy}(t) - y_{dy}(x=vt,t) - y_{st}(x=vt)] \\ &+ c_v[\dot{u}_{dy}(t) - \dot{y}_{dy}(x=vt,t) - \dot{y}_{st}(x=vt)] \\ &+ f(t)\ \ \delta(x-vt) \end{aligned} \tag{2}$$

where m_v, k_v, c_v, u are the mass, stiffness, damping coefficient, and total displacement of the vehicle, respectively; ρ, A, E, I, y_{st} are the density, sectional area, Young's modulus, moment of inertia, and the static displacement of the bridge, respectively; $\delta(x-vt)$ is the Dirac delta function; $u_{dy}(t)$ and $y_{dy}(t)$ are the dynamic displacement of vehicle and bridge, respectively.

Before deriving the displacement formulas, the nth mode frequency of the beam (ω_{bn}) with a mass m_s attached at the beam can be obtained using Rayleigh's method:

$$\omega_{bn}^2 = \frac{EI\int_0^L [y''_{st}(x)]^2 \mathrm{d}x}{\rho A\int_0^L [y_{st}(x)]^2 \mathrm{d}x + m_s[y_{stm,n}(L_s)]^2} = \Big[n^2\pi^2\sqrt{\frac{EI}{(\rho AL + 2m_s\sin^2(\frac{n\pi L_s}{L}))L^3}}\Big]^2 \tag{3}$$

where $y_{stm,n}(L_s)$ is the maximum deflection at L_s for the nth mode.

The displacement of bridge can be expressed in terms of the modal shape, $\phi_n(x)$, and modal coordinates, $q_{bn}(t)$, as:

$$y_{dy}(x,t) = \sum_{n=1}^{\infty} \phi_n(x) q_{bn}(t) = \sum_{n=1}^{\infty} \left[\sin \frac{n\pi x}{L} q_{bn}(t)\right] \tag{4}$$

By using the orthogonality conditions, for the nth mode, we have:

$$\begin{aligned}(\frac{\rho AL}{2} + m_s \sin^2(\frac{n\pi L_s}{L}))\Big\{&\ddot{q}_{bn}(t) \\ &+ \Big[n^2\pi^2 \sqrt{\frac{EI}{(\rho AL + 2m_s \sin^2(\frac{n\pi L_s}{L}))L^3}}\Big]^2 q_{bn}(t)\Big\} = \sin \frac{n\pi vt}{L} f_c(x = vt, t)\end{aligned} \tag{5}$$

Therefore,

$$\ddot{q}_{bn}(t) + \omega_{bn}^2 q_{bn}(t) = \frac{2}{\rho AL + 2m_s \sin^2(\frac{n\pi L_s}{L})} \sin \frac{n\pi vt}{L} f_c(x = vt, t) \tag{6}$$

where

$$\begin{aligned}f_c(x = vt, t) = &-m_v g + k_v[u(t)_{dy} - y_{dy}(x = vt, t) - y_{st}(x = vt)] \\ &+ c_v[\dot{u}(t)_{dy} - \dot{y}_{dy}(x = vt, t) - \dot{y}_{st}(x = vt)] + f(t)\end{aligned} \tag{7}$$

The solution of Eq. (6) can be calculated using a convolution integral

$$q_{bn}(t) = \frac{2}{\rho AL + 2m_s \sin^2(\frac{n\pi L_s}{L})} \int_0^t \sin \frac{n\pi v\theta}{L} f_c(v\theta, \theta) h_n(t - \theta) \mathrm{d}\theta \tag{8}$$

where $h_n(t-\theta)$ is the impulse response function for the nth mode:

$$h_n(t - \theta) = \frac{1}{\omega_{bn}} \sin \omega_{bn}(t - \theta) \tag{9}$$

Then, for the nth mode, the bridge displacement can be written as:

$$y_{dy,n}(x,t) = \frac{2}{\rho AL + 2m_s \sin^2(\frac{n\pi L_s}{L})} \sin \frac{n\pi x}{L} \int_0^t \sin \frac{n\pi v\theta}{L} f_c(v\theta, \theta) h_n(t - \theta) \mathrm{d}\theta \tag{10}$$

We can then transform Eq. (10) into the frequency domain:

$$Y_{dy,n}(x,\omega) = \frac{2}{\rho AL + 2m_s \sin^2(\frac{n\pi L_s}{L})} \sin \frac{n\pi x}{L} \mathcal{F}\Big\{\left[\sin \frac{n\pi vt}{L} \cdot f_c(vt, t)\right] * h_n(t)\Big\} \tag{11}$$

where, $\mathcal{F}\{f\}$ is defined as the Fourier transform of function f; $f * g$ is the convolution of f and g. In order to solve the Eq. (11), we need to use the convolution theorem:

$$\begin{aligned}\mathcal{F}\{f * g\} &= \mathcal{F}\{f\} \cdot \mathcal{F}\{g\} \\ \mathcal{F}\{f \cdot g\} &= \mathcal{F}\{f\} * \mathcal{F}\{g\}\end{aligned} \tag{12}$$

Thus, the frequency response of the displacement of the beam is obtained:

$$Y_{dy}(x,\omega) = \sum_{n=1}^{\infty} \frac{2\pi}{i(\rho AL + 2m_s \sin^2(\frac{n\pi L_s}{L}))} \sin \frac{n\pi x}{L} H_n(\omega) \cdot \Big[F_c(\omega - \frac{n\pi v}{L}) - F_c(\omega + \frac{n\pi v}{L})\Big] \tag{13}$$

where $H_n(\omega) = 1/(\omega_{bn}^2 - \omega^2)$; $F_c(\omega)$ is the frequency response of the contract force, and is defined as follows:

$$\begin{aligned} F_c(\omega) = -m_v g\sqrt{2\pi}\delta(\omega) + k_v[U_{dy}(\omega) - Y_{dy}(x = vt, \omega) - Y_{st}(\omega)] \\ + i\omega c_v[U_{dy}(\omega) - Y_{dy}(x = vt, \omega) - Y_{st}(\omega)] + F(\omega) \end{aligned} \tag{14}$$

where $U_{dy}(\omega)$, $Y_{dy}(x = vt, \omega)$ are the frequency response of displacement of vehicle and bridge, respectively; $Y_{st}(\omega)$ is the frequency response of the initial deflection of bridge.

Then, the mid-span acceleration of the bridge in the frequency domain can be written as:

$$\begin{aligned} \ddot{Y}_{dy}(\frac{L}{2}, \omega) = \sum_{n=1}^{\infty} \frac{2\pi m_v L^3 \omega^2}{i\pi^4 EI - i\omega^2 L^3(\rho AL + 2m_s \sin^2(\frac{n\pi L_s}{L}))} \sin(\frac{n\pi}{2}) \Big\{ \ddot{U}_{dy}(\omega - \frac{n\pi v}{L}) - \ddot{U}_{dy}(\omega + \frac{n\pi v}{L}) \\ + \sqrt{2\pi} g[\delta(\omega - \frac{n\pi v}{L}) \\ - \delta(\omega + \frac{n\pi v}{L})] \Big\} \end{aligned} \tag{15}$$

The n-th mode frequency response of the oscillator's acceleration is:

$$\begin{aligned} \ddot{U}_{dy,n}(\omega) = \ddot{U}_{dy,n}(\omega - \frac{2n\pi v}{L}) - \frac{i\pi^4 EI - i(\omega - \frac{n\pi v}{L})^2 L^3(\rho AL + 2m_s \sin^2(\frac{n\pi L_s}{L}))}{2\pi m_v L^3 (\omega - \frac{n\pi v}{L})^2 \sin(\frac{n\pi}{2})} \ddot{Y}_{dy,n}(\frac{L}{2}, \omega - \frac{n\pi v}{L}) \\ - \sqrt{2\pi} g[\delta(\omega - \frac{2n\pi v}{L}) - \delta(\omega)] \end{aligned} \tag{16}$$

From the derivation, we can draw the following conclusions:

- Non-linear property: Eq. (16) illustrates that the transformation from the severity mass to the amplitude of the acceleration signal's frequency response is non-linear.
- Uncertainty propagation: according to Eq. (16), different damage locations and severity levels only vary the term $S = m_s \sin^2(n\pi L_s/L)$. If we localize and quantify the damage severity step by step (a two-step model), the estimation of damage severity is: $m_s = S/\sin^2(n\pi L_s/L)$. Then the propagation of uncertainty from the damage location estimation can be calculated as follows:

$$\sigma_{m_s} = \pm\sqrt{\sigma_S^2 \frac{1}{\sin^4(n\pi L_s/L)} + \sigma_{L_s} \frac{4n^2\pi^2 S^2 \cos^2(n\pi L_s/L)}{L^2 \sin^6(n\pi L_s/L)}}. \tag{17}$$

  The sinusoidal function in the denominators makes the uncertainty of m_s very large, especially when the damage location is near the supports ($\|L_s - L/2\|$ is large). As a result, if a wrong damage location estimation appears, this error will propagate and consequence a wrong estimation of the damage severity level.

To overcome the problem of uncertainty propagation and preserve the non-linear property of the interactive VBI system, we propose a semi-supervised algorithm using MTL.

3.3 Semi-supervised Damage Location and Severity Estimation Algorithm using Multi-task learning

In practice, because of the lake of labeled examples, we want to achieve damage localization and quantification in a semi-supervised fashion, which generally needs to localize the damage first and then quantify the damage severity in the same location. However, as mentioned in the previous section, this 2-step method makes the uncertainty of the severity level estimation large and can result in an incorrect damage severity estimation. Thus, instead of a two-step model, we introduce a semi-supervised MTL model to localize and quantify the damage simultaneously with three tasks including reconstruction of input signals, damage location regression, and damage severity regression. The multi-task learning improves generalization by

leveraging the domain-specific information contained in the training signals of related tasks [16]. The architecture of our model is shown in Figure 3. For the first task (input reconstruction), we reduce the dimensionality of the fast Fourier transformation (FFT) outputs of acceleration signals by using stacked autoencoders with non-linear activation functions (ReLU). A stacked autoencoder is a neural network consisting of multiple layers of autoencoders to reconstruct its input. The encoder learns a representation z for a set of data x, and the decoder can reconstruct x from its encoding z. The architecture of our stacked autoencoder is $1936 \rightarrow 512 \rightarrow 16 \rightarrow 512 \rightarrow 1936$. For the second and the third tasks (damage severity estimation and localization), two regression layers are stacked on the bottleneck (or the 16-dimension feature layer) of the stacked autoencoder to predict damage location and severity. Furthermore, as a semi-supervised model, only a part of location and severity labels are given, which means that for the rest of the input signals that are unlabeled, the gradients of the second and the third task will be stopped during the training phase.

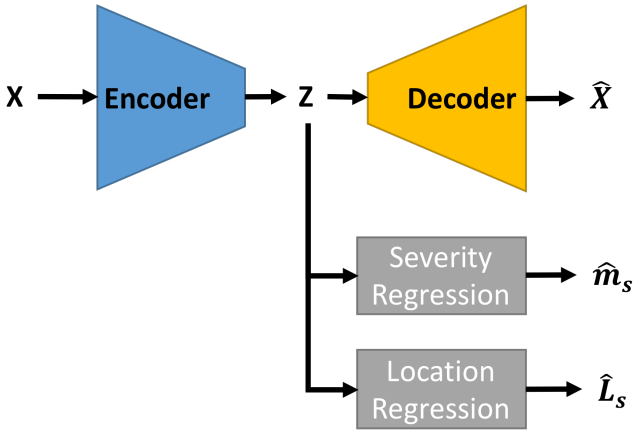

Figure 3. The architecture of the semi-supervised MTL model.

3.4 Experiments & Results

In this section, we use our semi-supervised MTL model to localize and quantify damage occurring on an experimental bridge. Figure 6 shows pictures of the experimental vehicle and the lab-scale bridge. The damage proxy is represented by adding mass at different locations on the bridge. A heavier mass means more severe damage since it appears as a more significant change from the initial condition. In this experiment, the mass ranges from 60 to 200 grams with an interval of 10 grams, so the attached mass varies from 0.38% to 1.29% of the mass of the bridge, which is 15.5 kg. For each severity level, the experiment is run at 3 different damage locations (the first quarter, the half and the third quarter of the bridge span), and for each damage scenario, the experiment is run 30 times. Furthermore, there are four accelerometers installed on the experimental vehicle, two of which are on the front and back chassis, and two on the front and back wheels. Thus, we have 15 (mass) $\times$ 3 (locations) $\times$ 30 (iterations) $=$ 1350 (trials), and 1350 (trials) $\times$ 4 (sensors) $=$ 5400 (signals).

In our study, we compare the performance of our MTL model with that of a 2-step model in damage localization and quantification. For the MTL model, we first train it with acceleration signals of lower and upper severity levels and their corresponding severity and location labels (severity from 60 grams to 90 grams and from 180 grams to 200 grams), and then predict the other damage locations and severity levels simultaneously. For the 2-step model, we first estimate damage locations using k-means clustering to partition 16-dimension features of FFT of acceleration signals learned by a stacked autoencoder into 3 clusters, and then we train regression models with the lower- and upper-severe acceleration signals in each predicted damage location (cluster), and then predict the other damage locations and severity levels. To

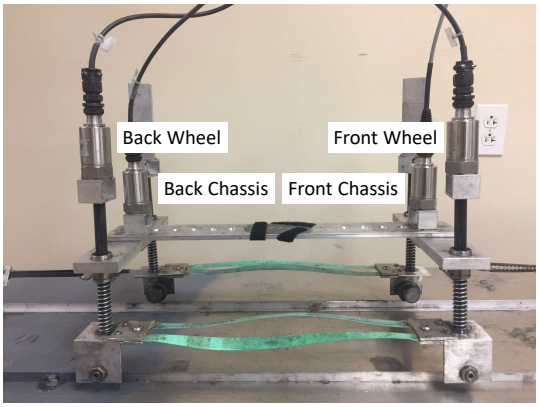

Figure 4. Vehicle.

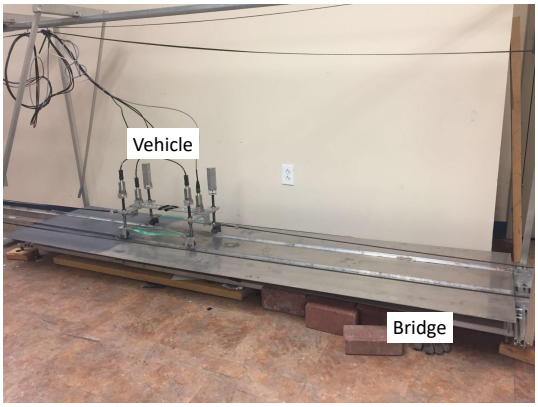

Figure 5. Bridge.

Figure 6. (a) Details of the passing vehicle and (b) the Lab-scale bridge under a moving vehicle.

evaluate these models, we calculate the root mean squared error (RMSE) between the predicted damage locations and severity levels with the corresponding labels. Figure 9 shows that in most cases our MTL model outperforms the 2-step model in terms of RMSE. In addition, even with a better damage location prediction, the damage severity prediction of the 2-step model is worse than that of the MTL model, which provides evidence of the problem of large uncertainty propagation from the location estimation.

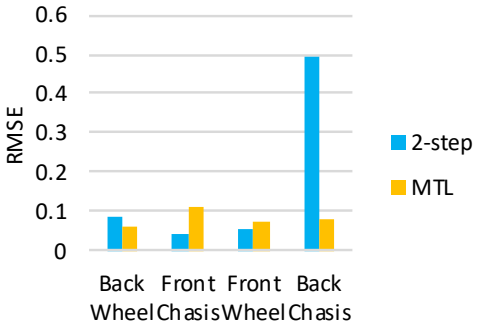

Figure 7. Damage location prediction.

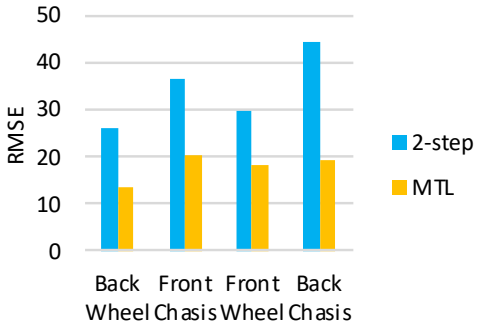

Figure 8. Damage severity prediction.

Figure 9. (a) Damage location and (b) severity prediction results using a 2-step method and MTL.

3.5 Conclusions

In this paper, we propose a semi-supervised damage localization and quantification algorithm using multi-task learning, which preserves the non-linear property of the VBI system and prevents from large uncertainty propagating from the damage location estimation. We evaluate our proposed model on an experimental dataset, and we show that it outperforms a two-step baseline model that localizes and quantifies the damage step by step. Our proposed model can estimate locations of the damage with an accuracy of 0.08 m (3.30% of the total length of the bridge) and changes in severity level with an accuracy of 17.81 grams (8.9% of the maximum severity mass). These results point to the applicability of indirect structural health monitoring with low cost and low maintenance.

4 Dynamic responses, GPS positions and environmental conditions of two light rail vehicles in Pittsburgh[2]

The previous section provides an understanding of the physical and mathematical aspects of a methodology for detecting gradual change in a structural model. In this and the next sections, we apply our damage diagnosis methodologies to a real-world dataset collected from light rail vehicles, and develop new approaches for improving their diagnosis capabilities.

Over the last five years, with the support of the UTC, we have collected an extensive data set from two light rail vehicles. In earlier projects, we addressed the difficulties associated with aligning the vehicle accelerations with the position data, and how to fuse signals from different sensor channels and different vehicles. In the present project, our group organized, validated, and released the collected data. This section provides a summary of the earlier work, as well as a description of the approach we followed to perform these tasks. Then, in Section 5, with the background of our earlier work, we describe a new approach we have developed for achieving indirect track geometry monitoring, which results in fewer false alarms than existing methods.

4.1 Background & Summary

The private freight rail industry in the U.S. makes $9.7 billion capital investment in maintaining the network, which is comprised of almost 140,000 miles of track and over 100,000 bridges in 2015 [17]. However, in 2017, the Federal Railroad Administration still reported 11,699 train accidents/incidents including 1,223 derailments and 470 track-caused accidents/incidents in the nation [18]. To ensure safety and reduce maintenance cost, it is necessary to develop low-cost and reliable techniques to monitor the status of railroad networks continuously, especially track geometries. In practice, two traditional approaches are usually adopted to inspect track infrastructure: (1) visual inspection and (2) inspection using a dedicated track geometry car. Visual inspection is neither reliable nor convenient. While inspection using a dedicated track geometry car can provide accurate track geometry data, it requires interruptions of regular train operations, and each inspection session has a more expensive cost than visual inspection. Due to its high cost and interruptions, it is difficult to conduct frequent inspections using a track-geometry car. In recent years, researchers have proposed many indirect track inspection methods using sensors, such as accelerometers and GPS, installed on in-service trains for track geometry monitoring and change detection [19, 20, 21, 22, 23, 24, 25, 26, 27] since it can be more reliable than visual inspection and costs less than inspection using a track-geometry car. Also, sensors installed on in-service trains can provide continuous monitoring of the track without affecting regular operations.

We monitored Pittsburgh's light rail network from sensors placed on passenger trains, as a more economical monitoring approach than either visual inspection or inspection with dedicated track vehicles. Over time, we learned how the trains respond to each section of track and use a data-driven approach to detect changes to the track condition relative to its historical baseline. We instrumented one train in Fall 2013, and a second train in Summer 2015. We have been continuously collecting data on the trains' position using GPS and their dynamic responses using accelerometers; in addition, our dataset includes environmental data as the trains were running on the track and the track maintenance logs from the light-rail operator.

Although there are some acceleration datasets for structure vibration testing [28], human activity recognition [29], senior fall detection [30] and gait recognition [31], at the time of writing, the DR-Train dataset is the only one to include multi-channel and high-frequency acceleration signals and GPS positions of light rail vehicles. The data were recorded from two light rail vehicles for four years with a variety of influential factors. This could be a benchmark dataset for comparing different vibration-based damage

[2]This work is based on the manuscript: Liu J., Chen S., Lederman G., Kramer D. B., Noh H. Y., Bielak J., Garrett J. H., Kovačević J., and Bergés M., Dynamic responses, GPS positions and environmental conditions of two light rail vehicles in Pittsburgh, Nature: Scientific Data, Submitted, 2018.

diagnosis algorithms. As a validation of our dataset, we have been able to detect changes in the tracks, which correspond to known maintenance activities. Besides detecting those changes, another usage of this dataset is for developing or validating data fusion methods. Data fusion methods integrate multiple data sources, such as multiple sensor channels on multiple light rail vehicles, to produce more consistent, accurate, and useful information than that provided by any individual data source. Our group has proposed a data fusion approach that integrates multiple accelerometers and GPS data sources from the same or different vehicles [27]. Also, the DR-Train dataset has many other potential usages. For example, environmental factors of each service run are logged in the dataset; researchers can reuse the dataset to investigate influences of the weather and temperature on the dynamic response of the light rail vehicles.

4.2 Methods

We use a data management system to collect and process dynamic responses and GPS positions of two passenger vehicles. We first introduce our monitoring target, the Pittsburgh Light Rail system, and our monitoring carrier, light rail vehicles in the following subsection.

4.2.1 The Pittsburgh Light Rail and instrumented Light Rail Vehicles

The Pittsburgh Light Rail, called the 'T' lines, is a 42.2-km light rail network in Pittsburgh, Pennsylvania. Figure 10 shows the transit map of the 'T' lines. This network is owned and operated by the Port Authority of Allegheny County (PAAC). It has 53 stations and around 28,000 daily ridership. The rail track, including street running track and ballasted track, in this network uses the Pennsylvania Trolley gauge rail whose track gauge is 1,588 mm. Also, the network contains bridges, viaducts, and tunnels, and is exposed to variable environmental conditions. For example, the temperature we observed ranges from -20°C to 35°C. The variety of influential factors makes it a viable test-bed.

A light rail vehicle (LRV) is a standardized vehicle for U.S. cities. LRVs of the Pittsburgh's light rail network have two models: Siemens SD-400 LRVs were built from 1985 to 1987 and assigned fleet numbers 4201 to 4255; Construcciones y Auxiliar de Ferrocarriles S.A. (CAF) LRVs were built from 2003 to 2004 and assigned fleet numbers 4301 to 4328. Those LRVs are supplied by a 650 voltage direct current electrification system. We installed accelerometers and GPS antennas on LRVs 4306 and 4313. These two trains are run in a two-car configuration with total length 25.810 m, empty weight 40 metric tons, total passenger capacity 264 and maximum speed 80 km/h.

4.2.2 Data management system

Our data management system consists of four key modules (as shown in Figure 11): Sensing module, data-acquisition module, data-storage module, and data-processing module.

Sensing module

Figures 12 and 13 show our instrumentations of two LRVs (fleet number 4306 and 4313). In 2013, we instrumented the LRV 4306 by placing two uni-axial accelerometers inside the cabin of the train (VibraMetrics 5102 [32]) and a tri-axial accelerometer (PCB 354C03 [33]) on the central wheel truck. The central wheel truck, or the central bogie, is a chassis attached to a vehicle and carrying wheelsets with a suspension system. Since it is not powered, the electrical noise is minimized. However, it has higher installation and maintenance costs than the system inside the cabin. For the second LRV instrumented (fleet number 4313) in 2015, we placed more sensors, including two uni-axial accelerometers (VibraMetrics 5102) and two tri-axial accelerometers (PCB 354C03) inside the train, for improving the system. To collect the position data, we placed a low-cost BU-353 GPS [34] antenna on the LRV 4306 and 4313. The GPS antenna in the LRV 4313 was installed within the interurban light enclosure for having a view of the sky. Tables 1 and 2 show important specifications of those sensors.

Data-acquisition and data-storage module

For data acquisition, we connected National Instruments USB-powered data acquisition hardware to a computer. Our data acquisition system samples acceleration signals at 1.6KHz and GPS position at 1

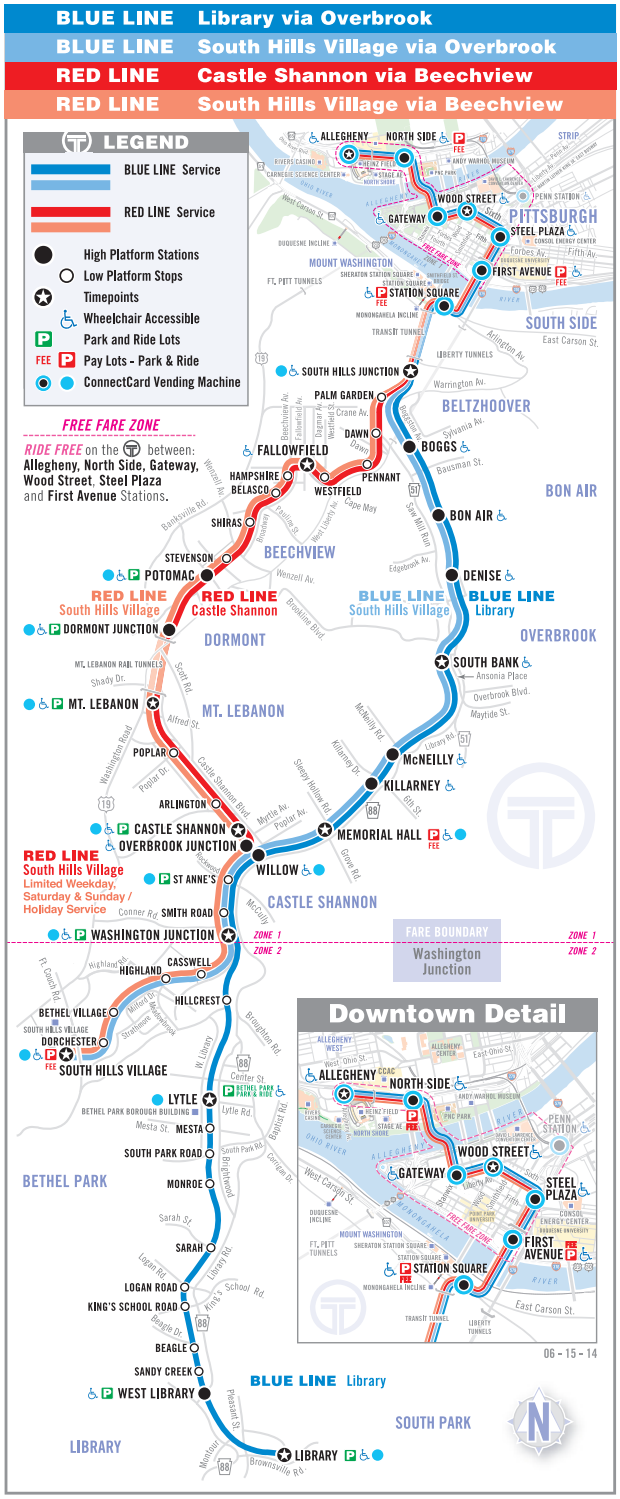

Figure 1 Pittsburgh light rail (the 'T' Lines) system map.

Hz and logs the data to an external hard drive. We downloaded the data manually from the onboard computers to our local computer every two weeks because we are not allowed to install wireless devices on LRVs. We use National Instruments LabVIEW [35] to control the hardware and acquire acceleration data.

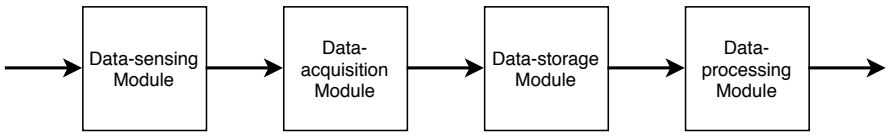

Figure 11. Proposed data-management system.

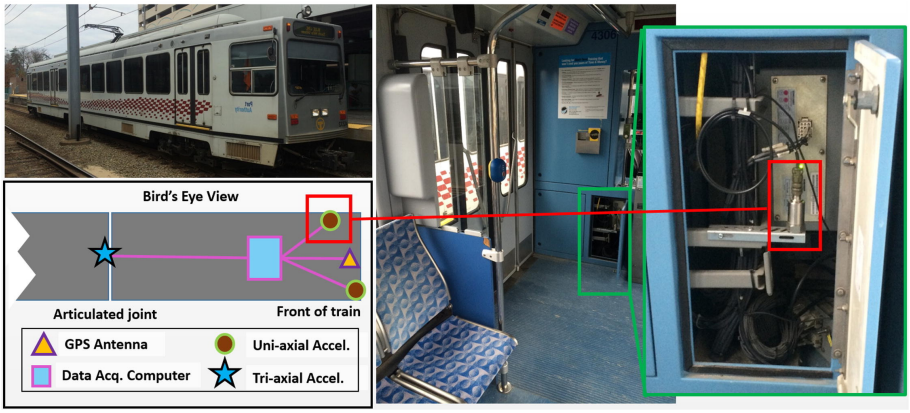

Figure 12. Data collection system of LRV 4306. Top left picture shows the exteral view of the LRV. Bottom left figure shows a schematic of the sensor locations on the LRV, and the inside view of the train and one highlighted uni-axle accelerometer are shown in the right hand side pictures.

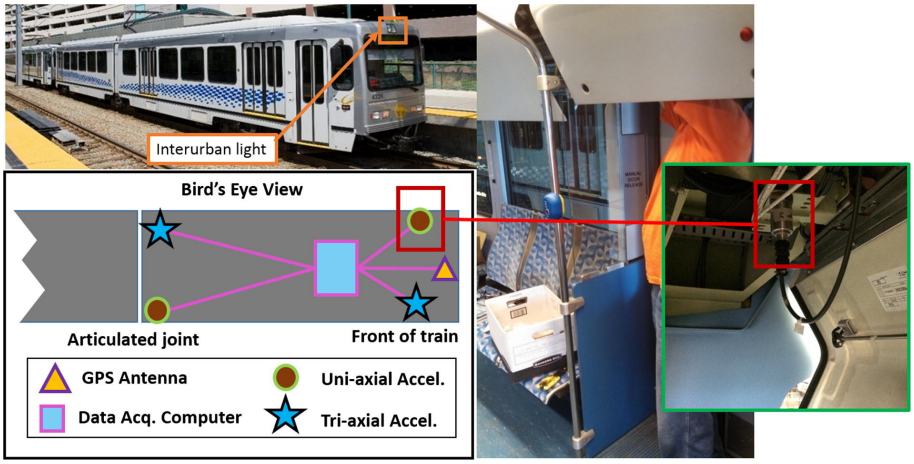

Figure 13. Data collection system of LRV 4313. Top left picture shows the exteral view of the LRV. Bottom left figure shows a schematic of the sensor locations on the LRV, and the inside view of the train and one highlighted uni-axle accelerometer are shown in the right hand side pictures.

Data-processing module

Before analyzing the collected data, it is necessary to segment it by geographical region. There are two reasons: first, we want to have the LRVs travel along the same path in each particular region; second, the GPS signal will be lost in tunnels, and it is difficult to determine the location of excitations. The rail network is divided into eight regions to ensure continuous GPS trace in each region. Figure 14 shows the GPS trace of several passes and the associated track regions.

The next step in processing the GPS data is to register it to a ground truth of the track position because the measurement error from collected GPS data could cause misalignment among different passes. PAAC provided us the foot by foot GPS position data, which allowed us to achieve this registration. We

Type	Model	No. of axles	Sensitivity	Amplitude range	Resonant Frequency
Piezoelectric Accelerometers	VibraMetrics 5102	1	500 mV/g (±5%)	±10 g	2.5 kHz
	PCB 354C03	3	500 mV/g (±10%)	±50 g	≥12 kHz

Table 1. Operating specifications of accelerometers.

Model	Number of channels	Sensitivity	Update rate	Accuracy
BU-353	48	-163 dBm	1 Hz	< 2.5 m

Table 2. Operating specifications of GPS receivers.

first utilized the iterative closest point (ICP) [36] algorithm to eliminate the global mismatch of the GPS data by minimizing the difference between every two GPS point clouds. Figure 15 show the GPS traces of 40 different outbound runs in the 5th track region before and after registration using ICP, respectively. For the local mismatch, the one-nearest neighbor algorithm is applied to register GPS position data of different runs to the nearest point of the ground truth GPS.

We also present environmental conditions and maintenance schedules during this monitoring period in the following sections.

4.2.3 Environmental conditions

Environmental conditions, including temperature, wind, weather, and precipitation, vary significantly when we collect the data. It is not only because all the sensors are sensitive to the operating temperature, but also steel rail expands as it heats up. To record the environmental conditions, we used the time stamp and the trains' GPS position to query environmental conditions from a weather data provider called Forecast.io (https://forecast.io/) when we were processing the collected data. This weather data provider gathered hour-by-hour environmental observations from tens of thousands of stations worldwide.

4.2.4 Maintenance schedules

Because we were not allowed to conduct an experiment on the track, we had to wait for changes made by PAAC's track maintenance. PAAC provides us with track allocation reports, which are stored in the DR-Train dataset as well. Those reports allow us to calibrate our data collection system and validate our track monitoring approaches.

4.2.5 Code availability

The code used to register GPS positions via ICP can be downloaded from MathWorks' file exchange [37]. The script and function used to load and process the data files can be downloaded from the online code repository. The codes have been tested using MATLAB 2017 on a typical personal computer and can run using different MATLAB versions and computers.

4.2.6 Known issues

- Even after GPS registration using ICP and one-nearest neighbor algorithms, misalignments of GPS positions and accelerations in the spatial domain still exist. This is because the GPS has variable accuracy levels at different locations.

- We found that the train's ventilation system is a source of noise. On a warm day, the air conditioner turns on, and there is higher energy at 30 Hz. Whereas on a cold day, the air conditioner turns off,

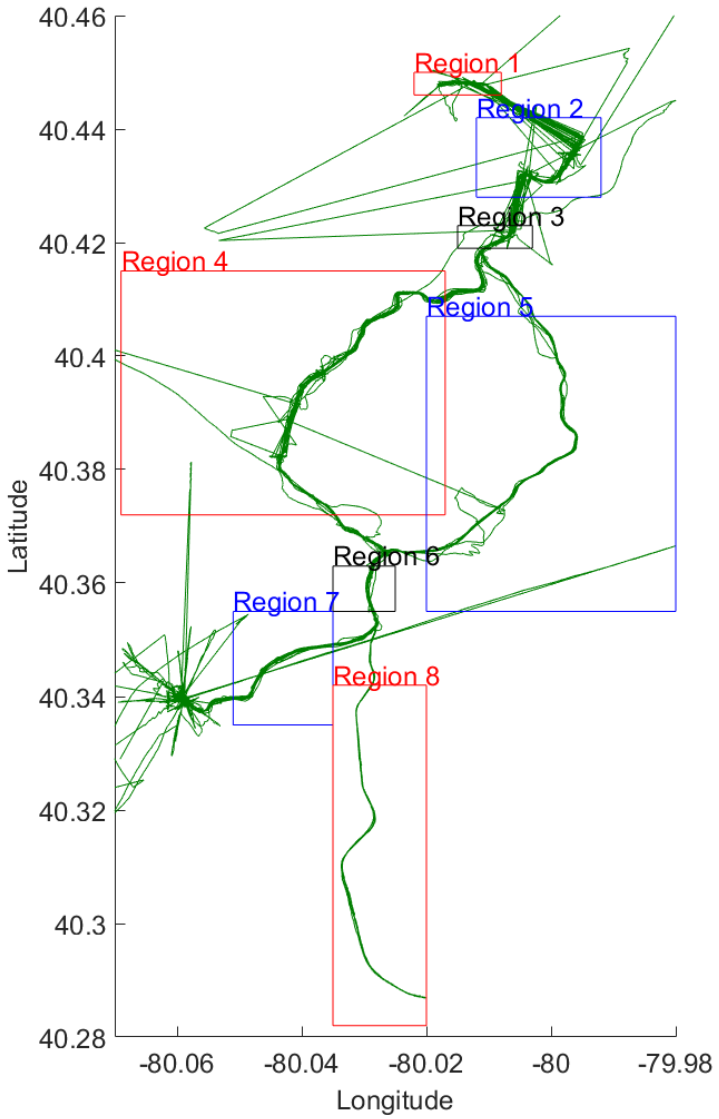

Figure 14. An example of the GPS trace of several passes through the 'T' lines and the associated track regions used for analysis.

so we observed less energy at 30 Hz. The signal energy at 30 Hz does not depend on the train speed or the track roughness.

- Individual sensors or sensor channels can be malfunctioning. Our group has developed a data fusion approach to address this problem [27].

4.3 Data Records

From 2013 to 2016, we collected acceleration and GPS position data with corresponding environmental conditions and maintenance logs. The DR-Train dataset includes 31 months of data from LRV 4306 and 11 months of data from LRV 4313. Table 3 shows the number of passes collected from the eight geographical regions mentioned in the Method section. 'Inbound' means that the LRV goes from South to North, and 'outbound' means the opposite direction. In some regions, the number of outbound passes is larger than that of inbound passes because, as the train emerges from the tunnel, there is a delay before the GPS can

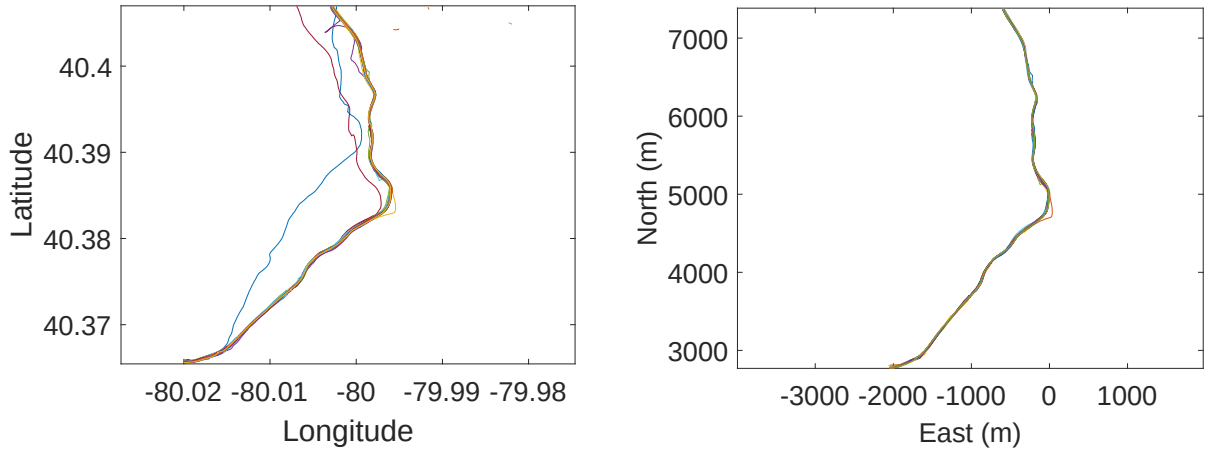

Figure 15. The GPS traces of 40 different outbound passes in the 5th track region before and after registation using ICP.

get a position lock.

All the data details and directories are stored in 'pass' MATLAB objects in '\data_files\LRV4306' and '\data_files\LRV4313' folders. The 'pass' object is defined in the MATLAB class function 'pass.m'. Properties and Methods of the 'pass' class are described in Table 4. For LRV 4306, there are 30,096 'pass' objects stored in the file '\data_files\LRV4306\obj_dict.mat'. LRV 4306 has five acceleration channels (property 'sensor'), corresponding to the two uni-axial accelerometers inside the train cabin and the three channels of the tri-axial accelerometer on the wheel truck. For LRV 4313, there are 18,929 'pass' objects stored in the file '\data_files\LRV4313\obj_dict.mat'. LRV 4313 has 8 acceleration channels (property 'sensor'), corresponding to the two uni-axial accelerometers and two tri-axial accelerometers inside the train cabin. The raw acceleration and GPS position data are stored in 'acceleration_data' and 'gps_data' folders. These data can be retrieved from files into the MATLAB/Octave workspace by loading acceleration filenames (property 'acc_raw') and GPS filenames (property 'gps_raw'). Each raw acceleration file only has a one-column MATLAB matrix in double-precision type, which is the logged temporal acceleration data of one single channel during one service run. Each raw GPS file has a five-column MATLAB matrix in double-precision type, corresponding to the longitude, latitude, altitude, velocity and time stamp during one service run. The time stamp is a serial date number that represents the whole and fractional number of days from a fixed, preset date ,January 0, 0000, in the proleptic ISO calendar.

Folder '\data_files\track_maintenance_logs' stores weekly maintenance schedule sheets from Light Rail System, PAAC. Those files provide information on what was happening on the rail network. Typically, the only work, which matters for this research, is done by the 'Way Department' that maintains the tracks.

This dataset is available from http://dx.doi.org/10.5281/zenodo.1432702.

4.4 Technical Validation

We validated the technical quality of the presented dataset from three perspectives. First, we consider a series of possible failure situations for the process of data collection and justify why we can rule them out; second, we consider a series of basic requirements that a high-quality dataset should satisfy and validate that the presented dataset satisfies all the requirements; third, a series of experiments have shown that changes to the tracks can be successfully detected based on the presented dataset.

4.4.1 Data Collection Failures

We consider the possible failure situations (missing data or corrupted data) as follows.

	LRV 4306		LRV 4313		
Region	Inbound	Outbound	Inbound	Outbound	Total
1	226	363	51	82	722
2	569	577	138	136	1420
3	579	567	135	131	1412
4	288	292	33	34	647
5	317	317	102	96	832
6	440	425	116	110	1091
7	356	342	85	80	863
8	180	182	65	63	490
Total	2955	3065	725	732	7477

Table 3. Number of passes collected from LRVs 4306 and 4313 through the eight geographical regions.

- The installed accelerometers fail to sense acceleration signals;
- The data-acquisition system fails to transfer acceleration signals to the installed computer;
- The installed computer fails to store the acceleration signals on the local disk;
- The data-processing system fails to organize acceleration signals correspondingly in the database.

Data visualization is an efficient way to rule out the first and the second failure situations. We added chart blocks in our LabVIEW implementation to visualize the collected acceleration signals instantaneously. We also plotted the collected data on our local computer. Figure 16 shows 27 properly collected spatial-domain acceleration samples of accelerometer channel 5 in geographical region 5 (outbound direction) during May 2014. By checking the size of logged data directly, we can rule out the third failure situation. Also, for this dataset, we rule out the top three failures by checking whether signals are sampled continuously with a constant sampling rate in the time domain. To rule out the fourth failure situation we have to download the data back to our local computer and validate the technical quality of them after data processing. The following section introduces two basic requirements of a high-quality dataset and their validations.

4.4.2 Basic requirements

We consider the basic requirements that a high-quality dataset should satisfy.

- R1: The acceleration signals collected from the same accelerometer channel should be consistent across trials during a period, such as one day, one week or one month. Since the acceleration signal of each trial reflects the roughness of the same track, the overall profiles of acceleration signals should be similar across trials. Otherwise, this dataset is problematic;
- R2: The acceleration signals should be correlated with the GPS positions. As a discrete-space signal, the acceleration signal of each trial is associated with the position of the track. For example, the amplitude of the acceleration signal around the train station should be low. Otherwise, this dataset is problematic;

Figure 17 and 18 show time periods (days) when sensors on LRVs 4306 and 4313 were recording. Blue lines indicate recording days, and white gaps indicate recording gaps in the dataset. The recording gaps are caused by one of three reasons: 1) Sometimes, the data-storage module runs out of space before downloading the data, and we are not allowed to install wireless sensors on the LRV in order to avoid interference between signals from our system and those of train control & communication systems; 2) The

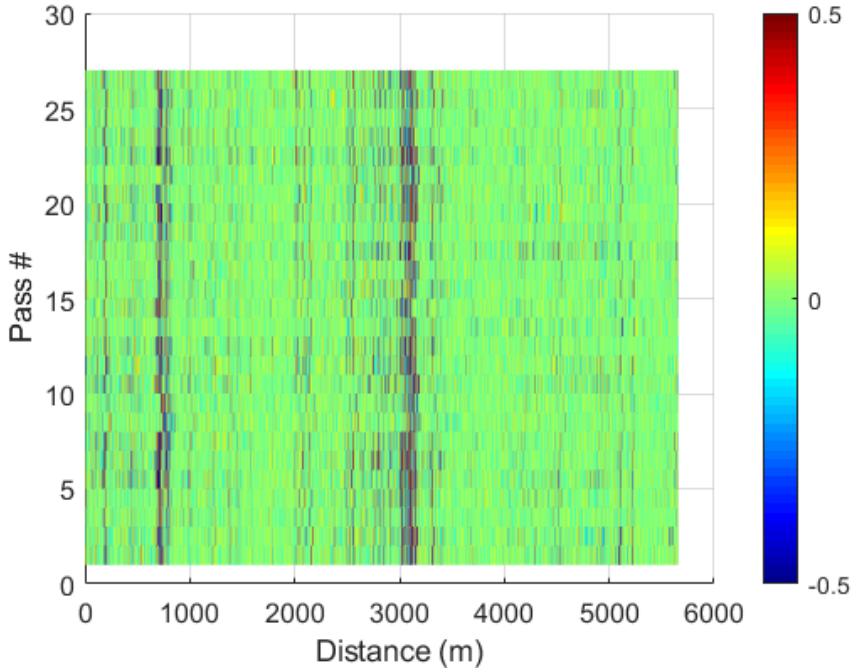

Figure 16. Visulizing acceleration samples in the spatial domain. We visualize the 27 acceleration samples of accelerometer channel five in region five during May 2014.

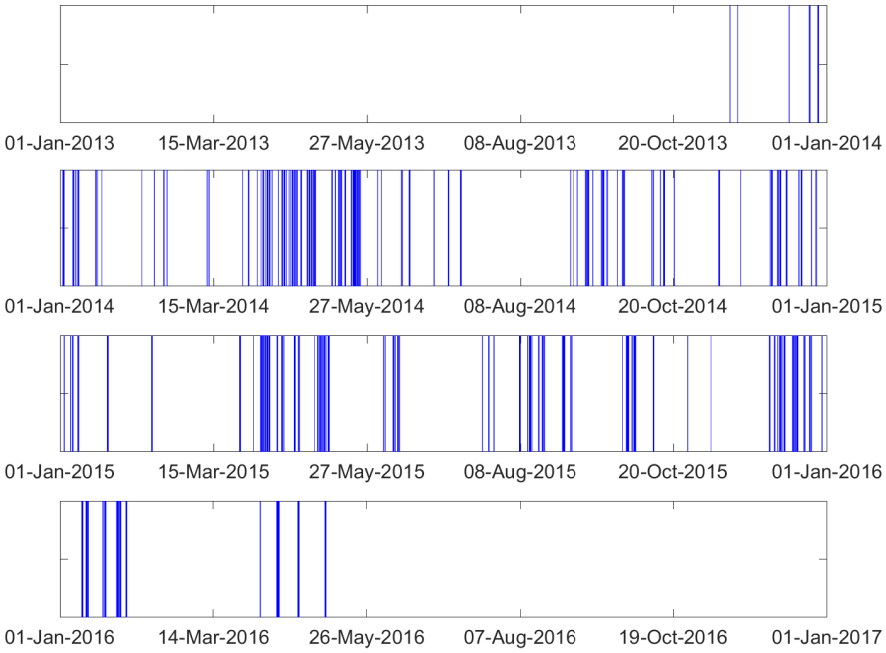

Figure 17. Time periods when sensors on LRV 4306 were recording. Blue lines indicate days when accelerometers and GPS were recording. The causes of recording gaps are explained in section 4.4.2.

data management system may not restart automatically after restarting the light rail vehicles, although we have programmed it to do that; 3) The light rail vehicles were not in service because of maintenance,

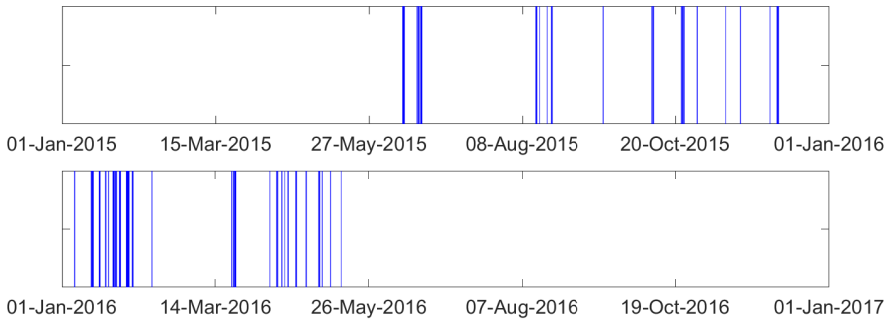

Figure 18. Time periods when sensors on LRV 4313 were recording. Blue lines indicate days when accelerometers and GPS were recording. The causes of recording gaps are explained in section 4.4.2.

inspection and repair.

Validation of R1

To prove the consistency of acceleration signals from the same accelerometer channel, we use the two-sample Kolmogorov–Smirnov test (K-S test) [38]. The two-sample K-S test is a general nonparametric method for comparing two samples. It quantifies a distance between the empirical distribution functions of two samples. The Kolmogorov–Smirnov statistic is

$$D_{n,m} = \sup_x |F_{1,n}(x) - F_{2,m}(x)|,$$

where $F_{1,n}$ and $F_{2,m}$ are the empirical distribution functions of the two samples, respectively, and sup is the supremum function. The null hypothesis that the samples are drawn from the same distribution is rejected at level if

$$D_{n,m} > c(\ )\sqrt{\frac{n+m}{nm}},$$

where n and m are the sizes of the two samples respectively, and for 5% and 1% rejection levels, $c(\ )$ is equal to 1.36 and 1.63, respectively.

The null hypothesis of our test is that the acceleration signals from the same sensor channel in the same time period and the same geographical region are drawn from the same distribution. The boxplot (Figure 19) shows a result of this test for LRV 4306. We randomly sample 1,000 acceleration amplitudes from each trail of the same sensor channel of LRV 4306 during May 2014 in region five. LRV 4306 ran 27 outbound trails during May 2014 in region five. We then calculate the K-S statistics of each pair of acceleration samples. For the tri-axle accelerometer installed on the central wheel truck (less electrical noise), the tests of the three channels are not rejected, both at 5% significance level and at 1% significance level. However, the two uni-axle accelerometers installed in the cabin are rejected at 5% significance level, but not rejected at 1% significance level.

Validation of R2

Because the trains were moving at different speeds, it is difficult to prove that every single acceleration and GPS position are correlated in the time domain. However, we can prove the geographical alignment of acceleration signals and GPS positions with the information of train stations. When arriving at a train station, the LRV stays stationary and idles. We assume that amplitude of the idling accelerations would be lower than the traveling accelerations due to the excitation of the tracks. Figure 20 shows two examples of acceleration and position data in Region 5. There are five stations in Region 5: Memorial Station (MS), Killarney Station (KS), South Bank Station (SS), Denise Station (DS), and Bon Air Station (BS). We can observe that the amplitude of the acceleration signal is small when the LRV was at stations, and the mileage stays the same at stations.

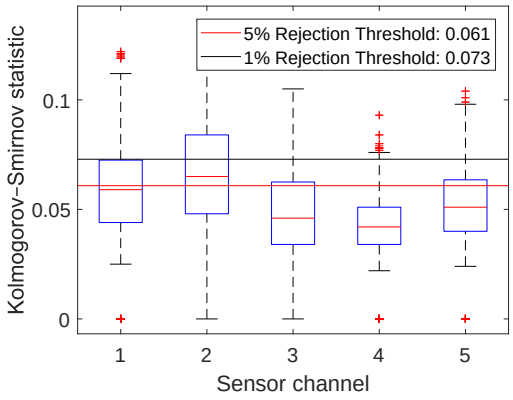

Figure 19. A result of the two-sample K-S test. For LRV 4306, there are 27 outbound trails during May 2014 in region five. We randomly sample 1,000 acceleration amplitudes from each trail and calculate the K-S statistics of each pair of samples. If the statistic is above the red line, the null hypothesis that two samples are drawn from the same distribution is rejected at level 5%. If the statistic is above the black line, the null hypothesis is rejected at level 1%.

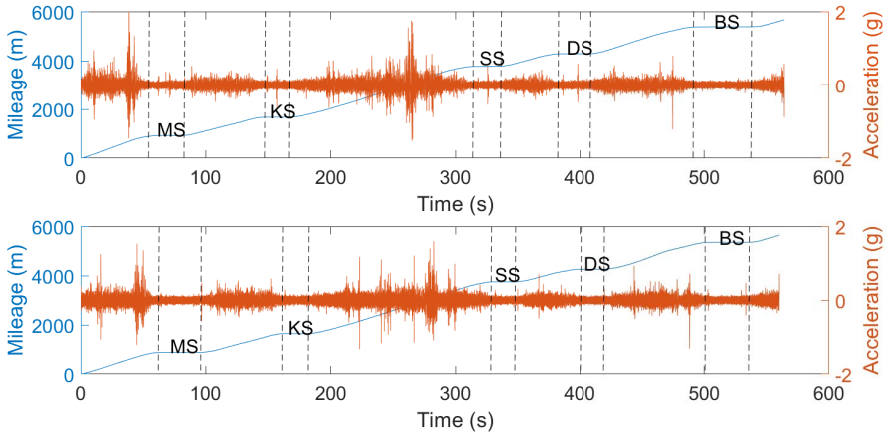

Figure 20. Two examples of acceleration and position data in region five. When the LRV was at those five stations: Memorial Station (MS), Killarney Station (KS), South Bank Station (SS), Denise Station (DS), and Bon Air Station (BS), the amplitude of the acceleration signal is small, and mileage stays the same.

4.4.3 Publications based on the presented dataset

Papers [25, 26, 27, 39] using the data described here have been published. Lederman et al. used the collected dataset to detect changes in the tracks, including changes in the tracks due to repair and changes in track geometry due to tamping, by applying implicit and explicit models. The implicit model first extracts different features from the raw acceleration signals and then performs change detection with some common methods, including cumulative sum chart control (CUSUM) [40], generalized likelihood ratio (GLR) [40] and Haar filter [41]. The explicit model solves for the parameters of the train's main suspension by enforcing sparsity in modeling the train system and learns where in the tracks the train is most excited by enforcing sparsity in the track profile. Lederman et al. [27] also proposed a data fusion approach for enabling data-driven rail-infrastructure monitoring from multiple in-service trains using the implicit model of the tracks.

4.5 Usage Notes

The data is provided in a MAT-file format with query files, and therefore it is convenient to load it in MATLAB. The script file (\code\main_script.m) calls the function (\code\load_processing.m) for loading and processing data and returns 'pass' objects, acceleration signals, and GPS positions.

5 Variational autoencoder for detecting anomalies in longitude elevation of track geometry using the dynamic response of an in-service train

Track geometry is the three-dimensional geometry of track layouts such as transverse elevations and longitudinal elevations, whose correct positions are of critical importance to ensure the safety of train operations. In this section, we propose a learning-based anomaly detection approach for monitoring longitude elevation of track geometry from the dynamic response of an in-service train. Also, we have validated this approach on the DR-Train dataset.

In general, the methods for estimating track geometry using acceleration data can be divided into two groups: model-driven methods [23, 42] and data-driven methods. In model-driven methods, there is usually a train-track interaction system that models the inverse relationship between vehicle acceleration and track geometry using prior knowledge about the system. However, the dynamics model depends on the characteristics of the train system, such as mass and the suspension system properties, which make model-driven methods susceptible to system characteristic uncertainties. For data-driven methods, Fourier Transform [22] and Wavelet [43] approaches are commonly employed to extract features from acceleration log and identify track geometry changes. However, data-driven methods, which rely much on the data, lack robustness to noise and require more physical insight for model selection and performance improvement.

It is worth noticing that both approaches mentioned above heavily rely on hand-crafted features. However, due to the noise in the collected accelerations, detecting anomalies using hand-crafted features often results in more false alarms. Many researchers have turned to learning-based methods to extract features from time-series signals automatically. Ordóñez et al. [44] used a many-to-one Long-Short-Term-Memory (LSTM) for wearable activity recognition. DiPietro et al. [45] proposed an LSTM-Conditional Random Field (CRF) model to extract features from raw acceleration signals for surgical activity labeling. Though learning-based methods obtained decent results in the activity recognition field, they might not be suitable for the geometry inspection problem for three reasons: (1) The acceleration signal is a direct measurement of the activity recognition application but an indirect measurement in the track inspection task. Therefore, acceleration signals recorded from an in-service train will contain more noise and will not directly reflect the track geometry. (2) activity recognition is a well-defined classification problem, but track geometry inspection is an anomaly detection problem, which is likely to have an imbalance distribution over normal samples and abnormal samples. (3) Directly using raw acceleration signals as input results in a high-dimension feature space, which can easily cause overfitting.

Considering the limitations of the LSTM-based methods, we turned to a variational autoencoder (VAE)-based anomaly detection method based on the insight of the underlying physical motion model. Through the solution of a single-mode differential equation of the motion model, we found that the spectrum of an acceleration signal is closely related to the spectrum of its corresponding track geometry. We considered the track geometry with a change as an anomaly, measured by the energy of the geometry slopes. The proposed method uses a VAE to detect anomalies. The VAE takes accelerations as input and learns a mapping from the frequency-domain of accelerations to a low-dimensional latent space that represents the distribution of the observed data. After the model is calibrated, the reconstruction probability of the input data is used as an anomaly score for indicating how well the input follows the normal pattern.

We validate the proposed VAE-based approach on the vibration data (DR-Train) collected from an in-service train that runs on a 42.2-km light rail network in the city of Pittsburgh, Pennsylvania. Figure 21 to 24 shows the results of our proposed method (VAE) with different anomaly thresholds for the energy of geometry slopes. It successfully addresses the overfitting problem presented in the LSTM-based methods and outperforms two supervised baseline models, a logistic regression model (Baseline) and a fully-connected neural network (NN-Feature), in terms of recall, precision, F1-score and area under the receiver operating characteristic (ROC) curve. The results outperform the other two methods and make the proposed indirect structural health monitoring approach a strong candidate for low-cost and frequent track

geometry inspection. Nonetheless, the authors identified three primary sources of error of the proposed approach: (1) GPS noise and drifting. Due to the noise from the GPS unit, acceleration signals from different passes are not well aligned with each other spatially; (2) Accelerometer noise. Accelerometers usually experience a high noise level that requires data denoising for acceleration data; (3) Asynchronous data. Data from different passes with different train velocities are collected asynchronously. In the future, we will concentrate on studying uncertainties of the model and improving its performance by adding physical constraints and prior knowledge.

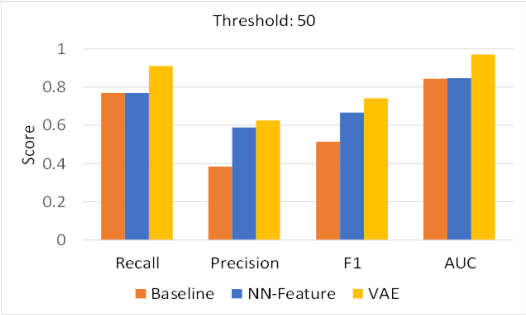

Figure 21. Recall, precision, F1-Score, and AUC with a 50 threshold of the energy of 4-second slopes.

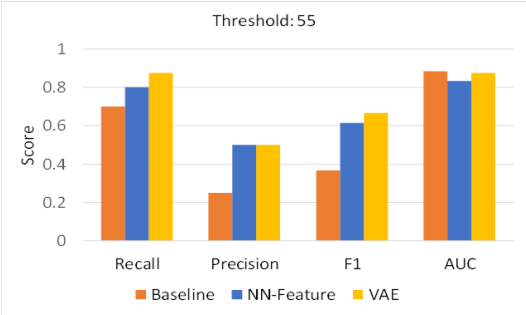

Figure 22. Recall, precision, F1-Score, and AUC with a 55 threshold of the energy of 4-second slopes.

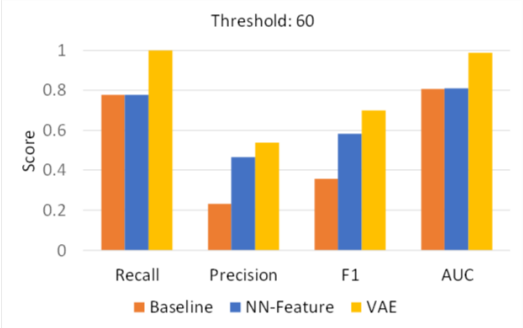

Figure 23. Recall, precision, F1-Score, and AUC with a 60 threshold of the energy of 4-second slopes.

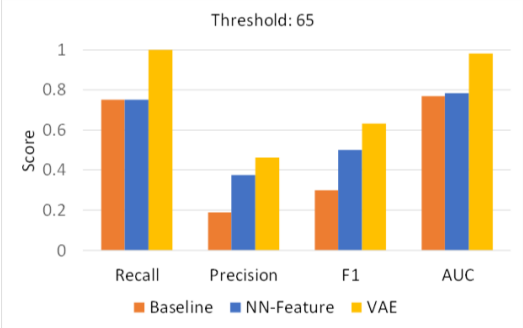

Figure 24. Recall, precision, F1-Score, and AUC with a 65 threshold of the energy of 4-second slopes.

6 Project Contributions

We have made contributions to indirect structural health monitoring, which is a low-cost and low-maintenance technology to monitor the rail and bridge infrastructure continuously.

Over the one-year project, we have developed and validated algorithms which are able to estimate, localize and quantify gradual changes in the infrastructure. We have investigated this problem in a theoretical way and conducted lab-scale experiments to prove the applicability of the indirect structural health monitoring. Signal processing and dimensionality reduction methods are used to achieve damage severity comparison, estimation, and localization with high accuracy. We hope we can continue to conduct on-site experiments and further studies for validating and consolidating the robustness of this damage diagnosis framework in the real world.

Also, we have contributed to released an open-access dataset recording dynamic responses from two in-service light rail vehicles that run on a 42.2-km light rail network in the city of Pittsburgh, Pennsylvania (USA). Our dataset also contains GPS positions and environmental data (including temperature, wind, weather, and precipitation) as the vehicles were running on the track and the track maintenance logs from the light-rail operator. We hope to publicize this dataset widely, which could inspire more research in this field, and allow us to understand the collected data better.

We have proposed a novel learning-based anomaly detection approach for monitoring longitude elevation of track geometry from the dynamic response of an in-service train. This approach overcomes limitations of model-based methods and methods using hand-crafted features, which are susceptible to characteristic uncertainties of the train-track interaction system and have many false alarms. It also outperforms conventional data-driven methods that use high dimensional time-domain accelerations as input and suffer overfitting for the track geometry anomaly detection problem. Our results as presented in section 5 make the proposed indirect structural health monitoring approach a strong candidate for low-cost and frequent track geometry inspection.

References

1. FHWA. Highlights from fhwa's 2017 national bridge inventory data (2017).

2. ASCE. 2014 infrastructure report card: Pennsylvania infrastructure grades (2014).

3. Yang, Y. & Lin, C. Vehicle–bridge interaction dynamics and potential applications. *J. sound vibration* **284**, 205–226 (2005).

4. Malekjafarian, A. & OBrien, E. J. Identification of bridge mode shapes using short time frequency domain decomposition of the responses measured in a passing vehicle. *Eng. Struct.* **81**, 386–397 (2014).

5. Kim, C.-W. *et al.* Experimental investigation of drive-by bridge inspection. In *5th International Conference on Structural Health Monitoring of Intelligent Infrastructure (SHMII-5), Cancun, Mexico, 11-15 December, 2011* (Instituto de Ingeniería, UNAM, 2011).

6. Lin, C. & Yang, Y. Use of a passing vehicle to scan the fundamental bridge frequencies: An experimental verification. *Eng. Struct.* **27**, 1865–1878 (2005).

7. Siringoringo, D. M. & Fujino, Y. Estimating bridge fundamental frequency from vibration response of instrumented passing vehicle: analytical and experimental study. *Adv. Struct. Eng.* **15**, 417–433 (2012).

8. Oshima, Y., Yamamoto, K. & Sugiura, K. Damage assessment of a bridge based on mode shapes estimated by responses of passing vehicles. *Smart Struct. Syst.* **13**, 731–753 (2014).

9. Malekjafarian, A. & OBrien, E. J. Identification of bridge mode shapes using short time frequency domain decomposition of the responses measured in a passing vehicle. *Eng. Struct.* **81**, 386–397 (2014).

10. Yang, Y., Li, Y. & Chang, K. Constructing the mode shapes of a bridge from a passing vehicle: a theoretical study. *Smart Struct. Syst.* **13**, 797–819 (2014).

11. Nguyen, K. V. & Tran, H. T. Multi-cracks detection of a beam-like structure based on the on-vehicle vibration signal and wavelet analysis. *J. Sound Vib.* **329**, 4455–4465 (2010).

12. McGetrick, P. & Kim, C. A wavelet based drive-by bridge inspection system. In *Proceedings of the 7th International Conference on Bridge Maintenance Safety and Management (IABMAS'14)* (2014).

13. Lederman, G. *et al.* Damage quantification and localization algorithms for indirect shm of bridges. In *Proc. Int. Conf. Bridge Maint., Safety Manag., Shanghai, China* (2014).

14. Chen, S. *et al.* Semi-supervised multiresolution classification using adaptive graph filtering with application to indirect bridge structural health monitoring. *IEEE Transactions on Signal Process.* **62**, 2879–2893 (2014).

15. Cerda, F. *et al.* Indirect structural health monitoring of a simplified laboratory-scale bridge model. *Smart Struct. Syst.* **13**, 849–868 (2014).

16. Caruana, R. Multitask learning. *Mach. learning* **28**, 41–75 (1997).

17. Association of american railroads. total annual spending: 2015 data (2015).

18. Federal railroad administration office of safety analysis. train accidents and rates (2017).

19. Caprioli, A., Cigada, A. & Raveglia, D. Rail inspection in track maintenance: A benchmark between the wavelet approach and the more conventional fourier analysis. *Mech. Syst. Signal Process.* **21**, 631–652 (2007).

20. Westeon, P. *et al.* Monitoring vertical track irregularity from in-service railway vehicles. *Proc. institution mechanical engineers, Part F: J. Rail Rapid Transit* **221**, 75–88 (2007).

21. Oshima, Y., Yamamoto, K., Sugiura, K., Tanaka, A. & Hori, M. Simultaneous monitoring of the coupled vibration between a bridge and moving trains. In *Proc. 5th IABMAS Conference, Philadelphia, USA*, 186 (2010).

22. Molodova, M., Li, Z. & Dollevoet, R. Axle box acceleration: Measurement and simulation for detection of short track defects. *Wear* **271**, 349–356 (2011).

23. Real, J., Salvador, P., Montalbán, L. & Bueno, M. Determination of rail vertical profile through inertial methods. *Proc. Inst. Mech. Eng. Part F: J. Rail Rapid Transit* **225**, 14–23 (2011).

24. Lee, J. S., Choi, S., Kim, S.-S., Park, C. & Kim, Y. G. A mixed filtering approach for track condition monitoring using accelerometers on the axle box and bogie. *IEEE Transactions on Instrumentation Meas.* **61**, 749–758 (2012).

25. Lederman, G. *et al.* Track-monitoring from the dynamic response of an operational train. *Mech. Syst. Signal Process.* **87**, 1–16 (2017).

26. Lederman, G. *et al.* Track monitoring from the dynamic response of a passing train: a sparse approach. *Mech. Syst. Signal Process.* **90**, 141–153 (2017).

27. Lederman, G. *et al.* A data fusion approach for track monitoring from multiple in-service trains. *Mech. Syst. Signal Process.* **95**, 363–379 (2017).

28. Wallace, J., Stewart, J. & Taciroglu, E. Field vibration testing and analytical studies of a four-story rc building (nees-2011-1074) (2017).

29. Micucci, D., Mobilio, M. & Napoletano, P. Unimib shar: A dataset for human activity recognition using acceleration data from smartphones. *Appl. Sci.* **7**, 1101 (2017).

30. Medrano, C., Igual, R., Plaza, I. & Castro, M. Detecting falls as novelties in acceleration patterns acquired with smartphones. *PloS one* **9**, e94811 (2014).

31. Zhang, Y. *et al.* Accelerometer-based gait recognition by sparse representation of signature points with clusters. *IEEE transactions on cybernetics* **45**, 1864–1875 (2015).

32. Mistras group, inc. product data sheet: Vibrametrics models 5102 (2013).

33. Pcb piezotronics mts systems corporation. model: 354c03.

34. Usglobalsat inc. usb gps receiver: Bu-353.

35. National instruments. labview (2012).

36. Bergström, P. & Edlund, O. Robust registration of point sets using iteratively reweighted least squares. *Comput. Optim. Appl.* **58**, 543–561 (2014).

37. Bergström, P. Matlab function for iterative closest point method.

38. Corder, G. W. & Foreman, D. I. *Nonparametric statistics: A step-by-step approach* (John Wiley & Sons, 2014).

39. Lederman, G., Noh, H. Y. & BIELAK, J. Rail-infrastructure monitoring through the dynamic response of a passing train. *Struct. Heal. Monit. 2015* (2015).

40. Gustafsson, F. & Gustafsson, F. *Adaptive filtering and change detection*, vol. 1 (Citeseer, 2000).

41. Vetterli, M., Kovačević, J. & Goyal, V. K. *Foundations of signal processing* (Cambridge University Press, 2014).

42. O'Brien, E. J., Bowe, C. & Quirke, P. Determination of vertical alignment of track using accelerometer readings. In *IMechE Stephenson Conference for Railways: Research for Railways, 21-23 April, 2015* (2015).

43. Bocciolone, M., Caprioli, A., Cigada, A. & Collina, A. A measurement system for quick rail inspection and effective track maintenance strategy. *Mech. Syst. Signal Process.* **21**, 1242–1254 (2007).

44. Ordóñez, F. J. & Roggen, D. Deep convolutional and lstm recurrent neural networks for multimodal wearable activity recognition. *Sensors* **16**, DOI: 10.3390/s16010115 (2016).

45. DiPietro, R. *et al.* Recognizing surgical activities with recurrent neural networks. In *International Conference on Medical Image Computing and Computer-Assisted Intervention*, 551–558 (Springer, 2016).

46. Esveld, C. Modern railway track: Digital edition (2015).

47. Kingma, D. P. & Welling, M. Auto-encoding variational bayes. *arXiv preprint arXiv:1312.6114* (2013).

	Name	Description
Properties	acc_al	address where aligned accelerometer data is stored
	acc_raw	address where accelerometer data is stored
	acc_samp	accelerometer sampling rate (Hz)
	count	this is the indice of the pass in terms of all passes
	date	date in UTC time
	datel	date string in local time
	daten	property date in 'datenum' format
	datenl	property datal in 'datenum' format
	direction	'inbound' our 'outbound'
	gps_al	address where aligned GPS is stored
	gps_raw	address where GPS is stored
	gps_samp	gps sampling rate (Hz)
	region	region on the map where the signal comes from
	sensor	number of sensor channel
	summary	weather summary text at time of pass
	summary8	weather summary text 8 hours prior to pass
	temp	temperature at the time of the pass
	temp8	temperature 8 hours prior to pass
	train	number of the train
Methods	addlistener	Add listener for event.
	addprop	Add dynamic property to MATLAB object.
	coor	show the coordinate system for the selected data
	date_bounds	This function take an array of passes, as well as lower and upper bounds for the dates (as strings), then plots the data that falls between the two specified date strings. Note this outputs the dates selected.
	delete	Delete a handle object.
	eq	== (EQ) Test handle equality.
	findobj	Find objects matching specified conditions.
	findprop	Find property of MATLAB handle object.
	ge	>= (GE) Greater than or equal relation for handles.
	gt	> (GT) Greater than relation for handles.
	isvalid	Test handle validity.
	le	<= (LE) Less than or equal relation for handles.
	listener	Add listener for event without binding the listener to the source object.
	lt	< (LT) Less than relation for handles.
	ne	= (NE) Not equal relation for handles.
	notify	Notify listeners of event.
	plot_both	Plot the data in time and frequency domain
	plot_freq	Plot the data in the frequency domain
	plot_gps	Plot the GPS trace on a map
	plot_time	Plot the data in the time domain
	scatter	Plot energy of the signal at the GPS points

Table 4. Properties and methods of the 'pass' class.